



# Observation of Alfvén Ion Cyclotron Waves in ICME Magnetic Clouds at 1 au

Omkar Dhamane<sup>1</sup>, Vinit Pawaskar<sup>1</sup>, Anil Raghav<sup>1</sup>, Zubair Shaikh<sup>2</sup>, Raffaella D’Amicis<sup>3</sup>, Kalpesh Ghag<sup>1</sup>, Kishor Kumbhar<sup>1</sup>, Daniele Telloni<sup>4</sup>, Georgios Nicolaou<sup>5</sup>, Prathmesh Tari<sup>1</sup>, Robert Wicks<sup>6</sup>, Utsav Panchal<sup>6</sup>, Bhagyashri Sathe<sup>1</sup>, and Prachi Pathare<sup>1</sup>

<sup>1</sup>Department of Physics, University of Mumbai, Mumbai, India; [raghavani1984@gmail.com](mailto:raghavani1984@gmail.com)

<sup>2</sup>Space Sciences Laboratory, University of California, Berkeley, CA 94720, USA

<sup>3</sup>National Institute for Astrophysics, Institute for Space Astrophysics and Planetology, Via del Fosso del Cavaliere 100, I-00133 Roma, Italy

<sup>4</sup>National Institute for Astrophysics, Astrophysical Observatory of Torino, Via Osservatorio 20, I-10025 Pino Torinese, Italy

<sup>5</sup>Department of Space and Climate Physics, Mullard Space Science Laboratory, University College London, Dorking, Surrey, RH5 6NT, UK

<sup>6</sup>Department of Mathematics, Physics and Electrical Engineering, Northumbria University, Newcastle upon Tyne, NE1 8ST, UK

Received 2023 June 23; revised 2023 July 28; accepted 2023 August 11; published 2023 October 25

## Abstract

Waves in plasma play an essential role in the energy transfer and plasma-heating processes. This article discusses the in situ observation of Alfvén ion cyclotron (AIC) waves and their characteristics within interplanetary coronal mass ejection (ICME) flux ropes. We analyzed 401 ICME flux ropes, observed by WIND spacecraft from 1995 to 2021 at 1 au. We found only five ICME flux ropes that show an explicit presence of AIC waves; two have normalized magnetic helicity  $\sigma_m \leq -0.5$ , and the remaining three show  $\sigma_m \geq 0.5$  polarization. The angle between velocity and magnetic field ( $\theta_{VB}$ ) for  $\sigma_m \leq -0.5$  is  $<40^\circ$ , whereas for  $\sigma_m \geq 0.5$ ,  $\theta_{VB} > 140^\circ$ . This result supports the existence of quasi-parallel and quasi-antiparallel left-handed polarized AIC waves within ICME flux ropes. We suggest that AIC waves are possibly triggered by (i) proton temperature anisotropy  $T_{p\perp}/T_{p\parallel} > 1$  driven by cyclotron instability and (ii) low-frequency Alfvén waves through the magnetohydrodynamic turbulent cascade. This study shows evidence of fluid and kinetic scales coupling in the ICME flux rope.

*Unified Astronomy Thesaurus concepts:* [Magnetohydrodynamics \(1964\)](#)

## 1. Introduction

Electromagnetic transverse waves with circular polarization, nearly field-aligned propagation, and frequencies close to the proton gyrofrequency ( $\Omega_p$ ) are known as ion cyclotron waves (ICWs; Stix 1962; Kindel & Kennel 1971). ICWs can originate from the free energy of ion species with velocities following distributions of large-temperature anisotropy ( $T_{p\perp}/T_{p\parallel} \gg 1$ ), where the temperature perpendicular ( $T_{p\perp}$ ) to the magnetic field is significantly higher than the temperature parallel ( $T_{p\parallel}$ ) to the field (Chang et al. 1986; Thorne & Horne 1994; Johnson & Cheng 1999; Telloni & Bruno 2016). Proton double streams and proton particle differential streams are examples of ion-beam distributions that may also contribute to the generation of right-handed magnetosonic waves or by altering the resonance condition for wave-particle interactions (see, e.g., Jian et al. 2009, 2014; Wei et al. 2016 and references therein). Pickup ions are linked to yet another potential mechanism for ICW wave generation (Jian et al. 2010). In addition, it is suggested that the high-frequency ICWs can be generated from low-frequency Alfvén waves through magnetohydrodynamic turbulent cascade (e.g., Tu et al. 1984; Hellinger et al. 2006; Telloni et al. 2019). The ICW in the solar wind was confirmed through measurements taken by spacecraft. These measurements revealed that ICW occurred within a frequency range of 0.01–10 Hz and amplitudes as large as  $\frac{\delta B}{B_0} \sim 0.4$ , where  $B_0$  is the background field strength (Behannon 1976; Tsurutani et al. 1994). It is believed that the resonant cyclotron interaction with ions could accelerate and heat the ions (Hollweg &

Turner 1978; Dusenbery & Hollweg 1981; Marsch & Tu 2001). Thus, ICWs are crucial for ion dynamics and plasma-heating processes in the solar wind and solar corona (Chang et al. 1986; Thorne & Horne 1994; Johnson & Cheng 1999; Marsch 2006; Telloni & Bruno 2016).

ICWs in the solar wind have been extensively studied (Jian et al. 2009, 2010, 2014; Wicks et al. 2016; Zhao et al. 2017, 2019). However, there are only a few studies that depict kinetic-scale waves inside the interplanetary coronal mass ejections (ICMEs) and in their substructures (Ala-Lahti et al. 2018, 2019). Coronal mass ejections (CMEs) are large-scale violent plasma eruptions from the solar atmosphere (Howard 2011; Webb & Howard 2012). The dynamics of space weather and the heliosphere are greatly affected by its interplanetary counterpart, the ICME (Zurbuchen & Richardson 2006; Knipp et al. 2011). Researchers have extensively examined their macrostructures in light of their impact on technology and science (Howard & Tappin 2009; Manchester et al. 2017). However, the microstates of ICMEs, particularly the wave-particle interactions that result in particle energization and/or kinetic processes, have not received adequate attention in the literature. Mirror-mode waves are present throughout the ICME sheath, from the shock to the magnetic cloud (MC) leading edge, but their amplitudes are greatest near the shock (Liu et al. 2006; Ala-Lahti et al. 2018). Moreover, ultralow frequency (0.01–0.05 Hz) waves and higher-frequency ( $\geq 1$  Hz) whistler precursors are observed upstream and downstream of ICME shocks (Kajdič et al. 2012; Kilpua et al. 2013; Blanco-Cano et al. 2016). In addition, Siu-Tapia et al. (2015) examined intricate formations resulting from the interaction between MCs and other transient events, utilizing measurements from STEREO. They observed the presence of both left-handed and right-handed low-frequency waves with near-circular polarization. (see, e.g., Siu-Tapia et al. 2015). The various in situ



Original content from this work may be used under the terms of the [Creative Commons Attribution 4.0 licence](#). Any further distribution of this work must maintain attribution to the author(s) and the title of the work, journal citation and DOI.

observations suggest the existence of Alfvén waves in ICME substructures, i.e., sheath and MC during CME–CME/CME–high-speed stream interactions (Raghav & Kule 2018a, 2018b; Raghav et al. 2018, 2019; Shaikh et al. 2019a; Dhamane et al. 2023a; Raghav et al. 2022, 2023; Dhamane et al. 2023b). However, how these waves dissipated in a flux rope structure remains an open question.

Alfvén ion cyclotron (AIC) waves refer to electromagnetic waves that propagate parallel to the magnetic field and have circular polarization; these waves encompass both low-frequency waves (Alfvén waves are waves far below the ion gyrofrequency) and high-frequency waves (ICWs are waves near the ion gyrofrequency; Davidson & Ogden 1975; Tajima et al. 1977; Ala-Lahti et al. 2019). Recently, Ala-Lahti et al. (2019) observed AIC waves within the ICME sheath region. They suggested that the occurrence of the AIC wave is highest near the shock front, whereas the rate decreases as we move closer to the ICME MC leading edge (Ala-Lahti et al. 2019). AIC waves are also observed in the Earth’s magnetosheath, where the occurrence frequency is high in the quasi-perpendicular bow shock at low Alfvén Mach number conditions (Schwartz et al. 1996; Remya et al. 2014; Soucek et al. 2015) and less frequent in the plasma depletion layer in the subsolar magnetosheath (Anderson et al. 1992; Soucek et al. 2015). Coleman (1968) suggested collisionless wave-particle scattering by AIC fluctuations as a possible explanation for high-temperature anisotropies. The presence of AIC waves greatly influences the heating of plasma in both the solar wind and the Earth’s magnetosphere (Roberts et al. 1990; Anderson et al. 1992; Hanson & Voss 2007). AIC waves have a variety of important consequences in multi-ion plasmas with relative drifts among the ion components—including parametric instabilities of the decay, beat wave, and modulational type (Hollweg et al. 1993)—substantial changes to the linear response of the systems (Gomberoff 2003; Araneda & Gomberoff 2004), and nonlinear ion-acoustic-like electro-static instabilities (Gomberoff et al. 2004).

In classical hydrodynamic turbulence theory, the energy cascade rate controls the commencement of the dissipation spectrum across the inertial range that drives dissipation (Eyink & Sreenivasan 2006). The spectrum responds to changing cascade and dissipation rates by adjusting the dissipation scale. However, measurements revealed that this does not hold true in the solar wind and, more likely, in most astrophysical plasmas (Alexandrova et al. 2013). The frequency break is a common feature observed in the power density spectra of the interplanetary magnetic field (IMF). This spectral break is believed to separate fluid-like fluctuations from kinetic-scale fluctuations (Telloni & Bruno 2016). Therefore, the links between these large- as well as small-scale space plasma fluctuation patterns across the frequency split are intriguing. (Bruno & Trenchi 2014). This break occurs around the proton kinetic scales, such as the proton inertial length and the proton Larmor radius (Telloni et al. 2015). In the literature, several models have been used to predict the precise frequency of the spectral break, but none of the models have yet been able to replicate the observations. Moreover, Bruno & Trenchi (2014) suggested the resonant condition for Alfvén/ICW, i.e., AIC wave provides the best agreement with observations. The AIC waves are frequently observed in turbulent solar wind (Franci et al. 2015) and are studied in the ICME sheath regions (Ala-Lahti et al. 2019). Moreover, the ICME flux ropes depict

different plasma characteristics than the surrounding solar wind or sheath regions (Kunow et al. 2006; Zurbuchen & Richardson 2006). However, no report has been found in the literature that discusses the generation of AIC waves in an ordered structure like ICME flux ropes.

The MHD scale fluctuations in collisionless plasmas can be dissipated via a turbulent cascade followed by various wave-particle interactions. The wave properties, wavevector direction, and anisotropy of the fluctuations transporting energy at tiny scales affect the energy separation between alpha particles, protons, and electrons and their heating efficiency (Maneva et al. 2015). Moreover, what role each type of wave plays in wave-particle interactions, anisotropic heating, and differential acceleration is a highly intriguing problem from an observational point of view. Numerical simulations demonstrated that the parametric instability of AIC waves in low  $\beta$  plasma could not be studied by ignoring the kinetic effects (Araneda et al. 2008). The reported studies suggested that the AIC waves are important candidates in studying solar wind plasma dynamics and its thermodynamics. Moreover, the ICME internal energetics are not well studied in the literature. This motivates us to investigate the existence and characteristics of AIC waves in the low  $\beta$  plasma of ICMEs. This will give an insight into the energy-exchange mechanism at the kinetic regime in ICMEs.

## 2. Data and Methodology

This study examined a total of 401 ICMEs MCs measured by the WIND spacecraft. The ICME catalog observed between 1995 and 2021 is available.<sup>7</sup> We use high-time resolution data from the Magnetic Field Instrument (MFI; 3 s and 92 ms; Lepping et al. 1995) and the Three-dimensional Plasma and Energetic Particle Investigation (3DP; 3 s) instrument (Lin et al. 1995) on board the WIND spacecraft. We specifically analyze the IMF strength ( $B_{\text{mag}}$ ), their components ( $B_x$ ,  $B_y$ ,  $B_z$ ), their elevation ( $\theta$ ) and azimuth ( $\phi$ ) angles, plasma proton density ( $N_p$ ), solar wind speed ( $V_p$ ), plasma temperature ( $T_p$ ), and plasma beta ( $\beta$ ) in Geocentric Solar Ecliptic coordinate system to detect the ICME events in the ambient solar wind at 1 au. Here, we focus on studying ICME MCs only. Each MC is identified using the following general criteria: (i) ordered and high magnetic field strength, (ii) low plasma temperature, (iii) very low plasma beta, and (iv) a gradual decrease in solar wind speed (Richardson & Cane 2004; Zurbuchen & Richardson 2006; Shaikh et al. 2020; Shaikh & Raghav 2022). We have also verified the ICME boundaries provided by the catalog as mentioned earlier.

Further, we have used fast Fourier transform to determine the total magnetic field power spectral density (PSD) and normalized magnetic helicity ( $\sigma_m$ ) for each identified ICME MC event (see Section 2.1). To explain the existence of significant wave-particle interaction, we applied criteria  $\sigma_m \geq |0.5|$  as suggested in Telloni (2020). A total of 14 ICME flux rope events out of 401 events listed in the catalog satisfied the above criteria. We aim to link the specific turbulence state within the inertial range of fluctuations to the polarization of magnetic field fluctuations at dissipative scales. The reported solar wind studies suggest the cyclotron resonance with Alfvén left-handed waves (Hollweg & Isenberg 2002; Marsch 2006). Thus, we search for left-handed magnetic waves. We applied the Walén test (see Section 2.2) to identify the Alfvénic fluctuations in these 14

<sup>7</sup> [https://wind.nasa.gov/ICME\\_catalog/ICME\\_catalog\\_viewer.php](https://wind.nasa.gov/ICME_catalog/ICME_catalog_viewer.php)

ICMEs' MCs. Interestingly, we found only five ICME MCs that show high Alfvénic fluctuations. We also estimate the angle between the IMF vector and solar wind velocity to identify wave propagation direction since solar wind speed is almost radial. Hence it is defined as  $\theta_{VB} = \theta_{BR} = \cos^{-1}(-B_x/B_{\text{mag}})$ . Below, we will briefly discuss the methods utilized in this study.

### 2.1. Power Spectral Density and Normalized Magnetic Helicity ( $\sigma_m$ )

To derive turbulence characteristics within ICME MCs, we used fast Fourier transformation on magnetic field data. Generally, a magnetic field's PSD follows power-law dependency as  $f^{-\alpha}$ , where  $f$  is the frequency and  $\alpha$  is the spectral index. In wavenumber space, the PSD of turbulent fluctuations is divided into three parts: injection range, inertial range, and dissipation range (Tu & Marsch 1995; Bruno & Carbone 2013; Kiyani et al. 2015). The different values of  $\alpha$  indicate different characteristics of turbulent and associated physical processes (see, e.g., Vlahos & Cargill 2009; Zimbardo et al. 2010; Horbury et al. 2012). Moreover, to determine the handedness (polarization) of each wave, we also derive the normalized magnetic helicity (Goldstein et al. 1994; Telloni et al. 2019; Telloni 2020)

$$\sigma_m(f) = \frac{2\text{Im}[Y^*(f) \cdot Z(f)]}{E_B}, \quad (1)$$

where  $f$  is the frequency;  $Y$  and  $Z$  are the Fourier transforms of the  $y$  and  $z$  components of the magnetic field vector in the geocentric solar ecliptic coordinate system; and the asterisk superscript indicates the complex conjugate. The parameter  $\sigma_m$  depicts the polarization of the magnetic fluctuations. It is zero for plane-polarized waves and  $\pm 1$  for right- and left-handed circularly polarized waves. Moreover, the direction of the background magnetic field strongly influences the sign of the normalized magnetic helicity (Telloni et al. 2012, 2013, 2019; Telloni 2020). The high speed of the solar wind ( $\gg V_A$ ) means that as the magnetic field rotates, the Doppler shift of the wave traveling over the spacecraft may change the sign of the measured helicity. Thus, it is essential to identify waves in the solar wind by a range of properties, such as correlations, frequencies and dispersion relations, and magnetic helicity. We used IMF data with an 11 Hz temporal resolution to estimate the PSD and  $\sigma_m(f)$ .

### 2.2. Walén Test

Alfvénic fluctuations are ubiquitous in space plasmas. Solar wind turbulence is frequently found to be Alfvénic. It is characterized not only by velocity-magnetic field correlations but also by low compressibility (almost constant magnetic field magnitude  $B$  and proton number density; Coleman 1968; Belcher & Davis 1971; Belcher & Solodyna 1975; Grappin et al. 1991). The Alfvén speed is defined as (Cramer 2011):

$$\vec{V}_A = \frac{\vec{B}}{\sqrt{\mu_0 \rho}}, \quad (2)$$

where  $\rho$  is the proton density,  $B$  is the magnetic field strength, and  $\mu_0$  denotes permeability of free space. To identify Alfvénic fluctuations in space plasma, we use the Walén test method,

which gives the relationship between Alfvén speed fluctuations and solar wind speed (Walén 1944; Yang & Chao 2013; Yang et al. 2016),

$$\overrightarrow{\Delta V} = R_w \overrightarrow{\Delta V_A}, \quad (3)$$

where  $R_w$  is the Walén slope,  $\Delta V = V_p - V_{\text{mean}}$  and  $\Delta V_A = V_A - V_{A \text{ mean}}$  are fluctuations in solar wind speed and Alfvén speed, respectively, and both fluctuations are determined by subtracting the averaged proton flow velocity ( $V_{\text{mean}}$ ) from measured values of plasma velocity ( $V_p$ ). Here, “mean” is the average value of the corresponding parameter in each interval under study. Ideally, a high correlation between the corresponding components of  $\Delta V$  and  $\Delta V_A$ , and  $R_w = \pm 1$  represents the equipartition of energy as predicted for ideal Alfvén waves.

Typically, the background quantities employed are either the mean values associated with specific regions or the averaged value within the de Hoffmann–Teller frame (Gosling et al. 2010; Yang & Chao 2013; Raghav et al. 2018). Nevertheless, according to Gosling et al. (2009) and Li et al. (2016), it has been argued that the de Hoffmann–Teller frame can undergo variations in high-speed solar wind streams and that the fluctuations in the solar wind are associated with a slowly changing base value of the magnetic field. It is shown by Li et al. (2016) that the fourth-order Butterworth bandpass filters are applied to each component of the plasma velocity and magnetic field data to decrease the uncertainty in Alfvén wave identification. Ten logarithmic frequency bands with equal spacing are chosen. The filters used are 10–15 s, 15–25 s, 25–40 s, 40–60s, 60–100 s, 100–160 s, 160–250 s, 250–400 s, 400–630 s, and 630–1000 s. Each band-passed signal's Walén relation is examined as follows (Shaikh et al. 2019b):

$$V_i = \pm R_w V_{Ai}. \quad (4)$$

The band-passed components  $V_i$  and  $V_{Ai}$ , which represent the filtered  $V$  and  $V_A$  values, respectively, are examined in this study. For each frequency band, the correlation coefficient between the corresponding components of  $V_i$  and  $V_{Ai}$  is calculated to determine whether Alfvén waves or Alfvénic fluctuations are present in the region under study. This technique is used, which is comparable to the method used by Li et al. (2016). A contour map of the frequency-time distribution with a bin size of 10 minutes is shown in Figure 3. Here, we have used WIND/3DP instrument data on the plasma and magnetic fields with a 3 s time resolution.

## 3. Event Analysis

The five ICME MC events with the signature of the AIC wave are listed in Table 1. In this section, we will describe one ICME MC event as a representative example.

Figure 1 shows the temporal variation (3 s temporal resolution) of plasma parameters and magnetic field during the passage of an ICME observed by the WIND spacecraft on 2000 July 31. We did not observe a clear ICME shock front and thus, sheath region. Moreover, the ICME MC crossover is depicted by the pink shaded region. Within the MC, the magnetic field is enhanced. It has smooth variations compared to the ambient solar wind field, slower variations in  $\theta$  and  $\phi$ , high plasma speed  $V_p$ , low proton density  $N_p$ , low plasma temperature  $T_p$ , and low proton plasma beta  $\beta$  (Zurbuchen &

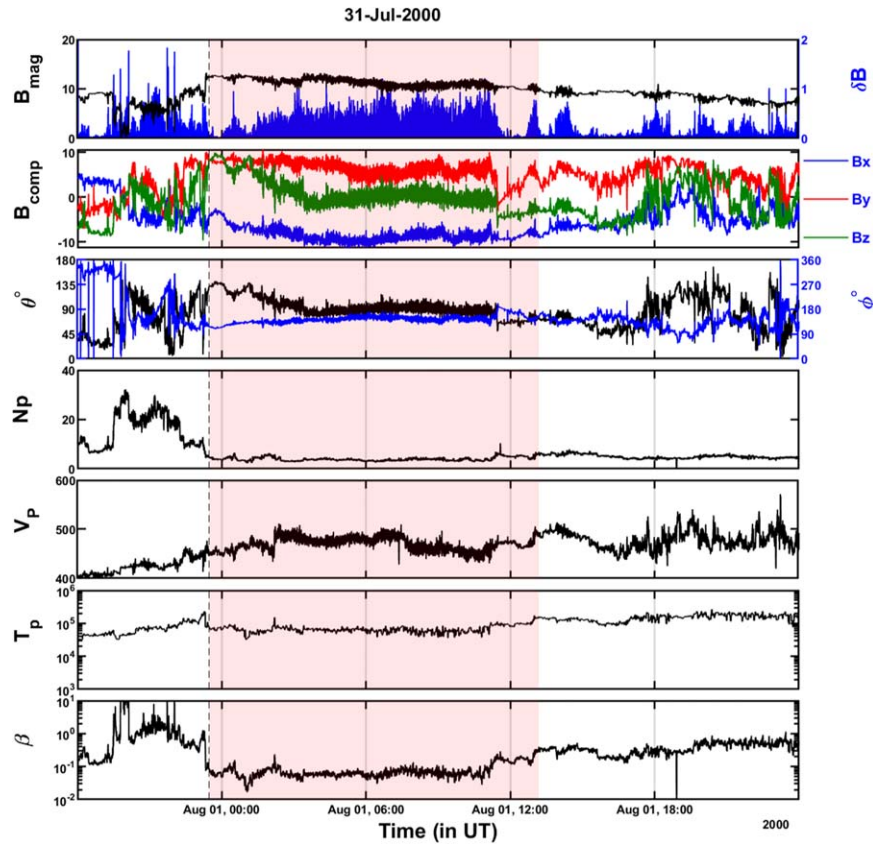


**Figure 1.** The interplanetary parameters correspond to the ICME’s transit (shaded area) on 2000 July 31, shown in the figure. The panels from top to bottom represent total IMF ( $B_{\text{mag}}$  in nanotesla), the absolute value of IMF fluctuation, i.e.,  $\delta B_i = \frac{B_{i+1} - B_{i-1}}{2}$ ; IMF vector components, i.e., ( $B_{\text{comp}}$ ); azimuth ( $\phi$ ), and elevation ( $\theta$ ) angle; proton density ( $N_p$  in centimeters cubed); plasma velocity ( $V_p$  in kilometers per second); temperature ( $T_p$  in kelvins); and plasma beta ( $\beta$ ).

**Table 1**  
A List of Events in Which We Found AIC Waves

ICME Start Time	MC Start Time	ICME End Time	$\theta_{\text{VB}}$	Nature of Fluctuations
1999 02 18 02:48	1999 02 18 09:14	1999 02 19 00:00	140°26	Quasi-antiparallel
2000 06 08 09:07	2000 06 08 16:47	2000 06 10 01:18	26°58	Quasi-parallel
2000 06 23 12:57	2000 06 24 09:00	2000 06 25 23:58	145°54	Quasi-antiparallel
2000 07 31 23:28	2000 07 31 23:28	2000 08 01 13:11	39°90	Quasi-parallel
2014 06 22 18:28	2014 06 22 18:28	2014 06 23 22:04	147°01	Quasi-antiparallel

**Note.** Respective mean  $\theta_{\text{VB}}$  values and their nature concerning the background magnetic field are also included. The start and end time taken from [https://wind.nasa.gov/ICME\\_catalog/ICME\\_catalog\\_viewer.php](https://wind.nasa.gov/ICME_catalog/ICME_catalog_viewer.php).

Richardson 2006; Shaikh & Raghav 2022). The onset of the MC is on 2000 July 31 at 23: 28 UT. We also noticed higher  $\delta B$  fluctuations superposed on total IMF during the MC passage.

Figure 2 demonstrates the PSD plot of  $B_{\text{mag}}$  and  $\sigma_m$  for the MC interval. Here, we observed the three humps in the PSD plot near frequencies at  $\sim 0.1$  Hz, 0.60 Hz (close to the proton gyrofrequency), and 1.24 Hz. We estimated the gyrofrequency of protons by considering the average total IMF of the flux rope and depicted all the above-mentioned frequencies using a vertical dotted line. We noted that the average  $\sigma_m$  is  $< -0.5$ . Interestingly, we also observed humps in PSD (Jian et al. 2009) exactly match a bump in the  $\sigma_m$  curve as in Telloni et al. (2019). The peak in the  $\sigma_m$  spectrum is a robust signature of parallel-propagating left-handed polarized ICWs. However, ICWs at proton scales are related to the amplitude of the turbulent fluctuations (Telloni & Bruno 2016). This spectral

break around the gyrofrequency could link fluid and kinetic scales in MC.

Furthermore, to identify the presence of Alfvénic fluctuation, we applied the Walén test during the passage of the MC. The top three panels in Figure 3 represent the Walén test result for this event, indicating a significant positive correlation between all three components of  $V$  and  $V_A$ . It confirms the Alfvénic nature in ICME MC. The  $\theta_{\text{VB}}$  is consistently found near  $40^\circ$  (refer Figure 3) during the MC interval. The observations of the coexistence of Alfvénic mode with ICWs may support the left-handed polarized (negative) quasi-parallel flow of the AIC wave (He et al. 2011a; Telloni 2020). Further, we found high-temperature anisotropy  $T_{p\perp}/T_{p\parallel}$  during the passage of ICME MC. We performed an analysis similar to the rest of the four ICME MCs that exhibit strong signatures, and we found similar results, which we list in Table 1.

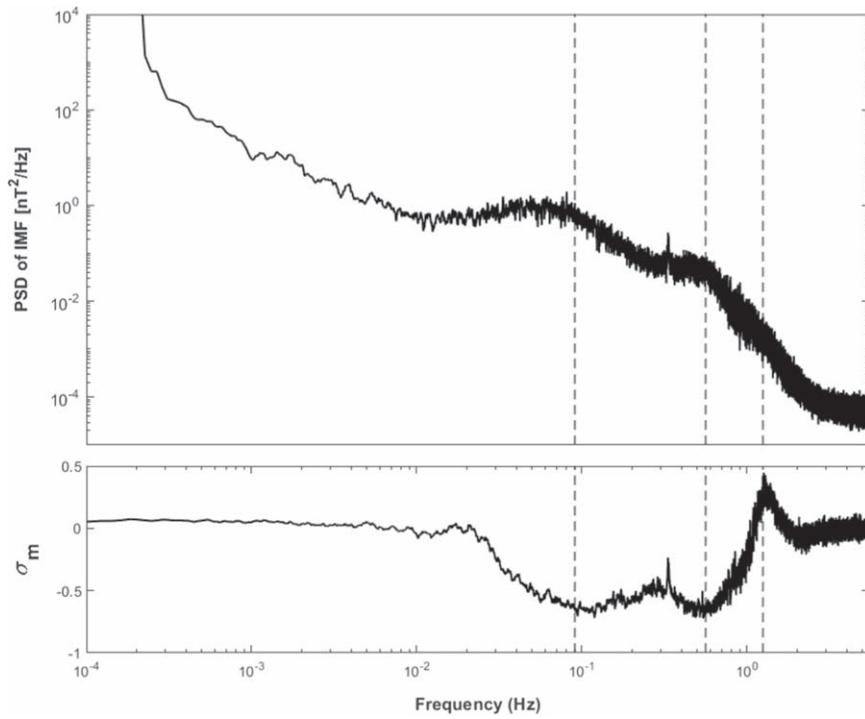


**Figure 2.** PSD of  $B_{\text{mag}}$  and  $\sigma_m$  for MC is plotted. The 11 Hz magnetic field data of the WIND spacecraft instruments are used for estimation.

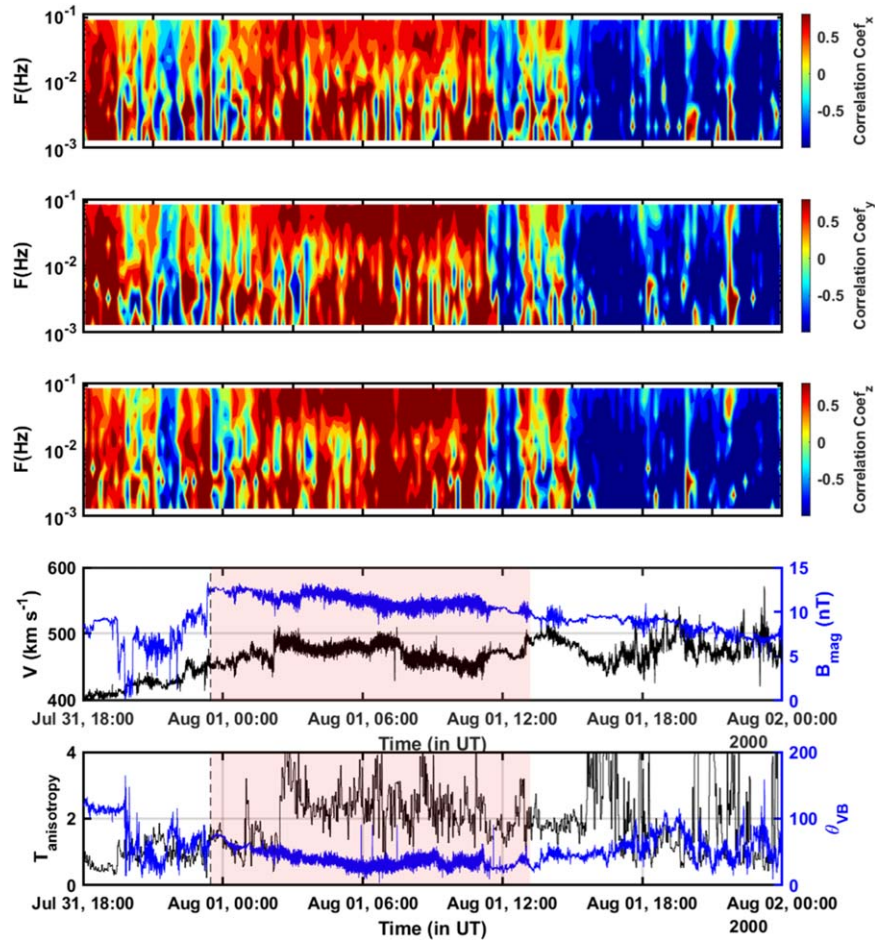


**Figure 3.** Time-frequency distribution of correlation coefficients between  $V_{A_i}$  and  $V_i$  for the entire event. Solar wind speed and magnetic field are shown in the fourth panel. Temperature anisotropy and  $\theta_{VB}$  are plotted in the last panel. WIND satellite 3 s observations from MFI and 3DP, in addition to the Solar Wind Experiment (92 s; Ogilvie et al. 1995) for temperature anisotropy are utilized for the analysis.

#### 4. Discussion

In general, the Alfvénic turbulence inside ICME flux ropes is a low-amplitude, i.e., weak turbulent. However, the example shown (see Figure 1) includes high-frequency fluctuations in total IMF, with left-handed polarization and high Alfvénicity; hence, we identify them as AIC waves. The high-frequency fluctuations are not visible at the front and back ends of the flux rope. It implies that the outer layer of the ICME flux rope is free of these high-frequency fluctuations. As a result, we conclude that the shear interaction between the solar wind and flux rope is not responsible for the observed superposed high-frequency fluctuations in the flux rope. In fact, we are unaware of the source of such significant fluctuations in the flux rope to date. Moreover, the microstate examination of ICME flux ropes has been overlooked in past studies. A thorough, dedicated investigation is required to get insight into the local processes and couplings in flux rope plasma that trigger instabilities and may influence the overall evolution of ICME in the heliosphere. Thus, we investigate the prototype event in the light of MHD and kinetic-scale coupling.

The Elsässer variables ( $z^\pm$ ) can be used to study the Alfvénic content of the fluctuations. It is defined as  $z^\pm = v \pm b$  where  $v$  is the velocity and  $b$  is the magnetic field vector in Alfvén units (Tu et al. 1989; Grappin et al. 1991). We derive the residual energy  $\sigma_R$  from the total energy and particularly focus on the cross helicity. The  $e^\pm$  is the energy defined using the  $z^\pm$ . The normalized cross helicity is given by the formula  $\sigma_c = (e^+ - e^-)/(e^+ + e^-)$  and the normalized residual energy as  $\sigma_R = (e^v - e^b)/(e^v + e^b)$ . Here,  $e^v$  is the trace of the spectra of the velocity components, while  $e^b$  is the trace of the spectra of magnetic field components in Alfvén units. As  $\sigma_c$  and  $\sigma_R$  are normalized, they will vary from  $-1$  to  $1$ .

The power spectra for velocity and magnetic field can be used to characterize solar wind fluctuations. Particularly, the balance between  $z^+$  and  $z^-$  is shown by  $\sigma_c$ , whereas  $\sigma_R$  represents the state of equipartition between magnetic and kinetic energy. Figure 4 demonstrates the PSD of the trace of magnetic field ( $\text{PSD}(B_x) + \text{PSD}(B_y) + \text{PSD}(B_z)$ ),  $e^+$ ,  $e^-$ ,  $e^v$ , and  $e^b$ . In addition, we determined the  $\sigma_c$  and  $\sigma_R$  in the frequency domain using 3 s data. Note that the PSD of the trace of the magnetic field is estimated with 11 Hz data. Here, we examine the highly fluctuating ICME MC region from 02:15 UT to 11:30 UT on 2000 August 1. The left panel of Figure 4 depicts the PSD of the total magnetic field with three spectral breaks shown by the vertical dashed line. These three spectral breaks corroborate the outputs of Figure 2.

The PSD of  $e^v$  and  $e^b$ , as shown in the right top panel of Figure 4, demonstrates a distinct equal distribution for both energies. The  $\sigma_R$  values fluctuating near zero confirms a strong resemblance to Alfvénic characteristics. The middle top panel of the same figure demonstrates a similar hump in  $e^-$  PSD spectrum as that of  $e^v$  and  $e^b$ . However, the PSD of  $e^+$  shows flat distribution.  $\sigma_c$  reaches  $\sim -1$  at the same frequency corresponding to the leftmost hump in Figure 4(a), which might be interpreted as inward Alfvénic fluctuations although it should be investigated in more detail. The above estimation deduced that the inward-directed Alfvénic turbulence dominates near the first spectral break of Figure 4(a). It further implies a higher rate of dissipation/exchange of energy at the bump frequency region. Moreover, what is the reason for the inward turbulent flow being more dominant than the outward

flow in the ICME MC? This is an exciting research question for the future.

Moreover, Grappin et al. (1982), Roberts et al. (1987), and Bruno & Carbone (2013) suggested that  $\sigma_R$  has a tendency to vanish in the Alfvénic range. For higher frequencies,  $\sigma_R$  has an imbalance in favor of kinetic energy usually associated with the noise of velocity spectra. The middle hump corroborates fluid and kinetic-scale coupling near the gyrofrequency (0.6 Hz). It is expected that decreasing the Alfvénicity leads to the energy exchanges between magnetic and kinetic energy, resulting in the heating of protons.

To confirm our observations, we measured the spectrum  $\sigma_m$  with respect to the local mean magnetic field at various angles, allowing one to roughly analyze  $\sigma_m$  as a function of the wave propagation direction (He et al. 2011a; Podesta & Gary 2011a, 2011b). The spectrum  $\sigma_m$  for each vertical slice is presented at an angle  $\theta_{VB}$  with respect to the direction of the local mean magnetic field. When observing fluctuations while looking roughly parallel to angles  $B_{\text{mag}}$ , a population of fluctuations with left-hand polarization is seen. In Figure 5 (plotted with 11 Hz data), we observed that at or near gyrofrequency, i.e.,  $k\rho \sim 1$ , the helicity has a maximum negative value, and the angle is below  $40^\circ$ . It has been inferred that the quasi-parallel fluctuations are AIC waves moving away from the Sun. It is attributed to wave energy transferred to the ion scales by kinetic microturbulence. The turbulent Alfvénic fluctuations interact with protons at frequencies close to gyrofrequency via resonant ion cyclotron scattering. This process results in the release of energy across the magnetic field direction. The magnitude of the magnetic fluctuations within the inertial range would therefore be linked to the degree of temperature anisotropy (see Figures 3). The particle velocity distribution function is altered by the anisotropy in the system, which reshapes it. This anisotropy is responsible for the successive release of free energy by generating AIC waves. Plasma instabilities form to produce waves that dissipate excess (perpendicular) energy. The significant departure from an isotropic, thermal equilibrium causes the plasma to become unstable, which causes waves to be produced as a means of dissipating the extra (perpendicular) energy (Gary et al. 1994; Telloni et al. 2019).

We utilized the estimation of magnetic helicity and PSD of IMF to uncover the nature of the turbulence at the kinetic scale in the ICME flux rope. We observed an explicit hump in the PSD spectrum of all the IMF components for each listed event in Table 1. The study found a strong positive/negative magnetic helicity (values greater than 0.5 or smaller than  $-0.5$ ) within the proton gyrofrequency range of about  $0.9 < k\rho_i < 1.1$ , where  $\rho_i$  is the proton gyroradius. Furthermore, we found a high correlation coefficient between the magnetic field components and the solar wind velocity vector. It indicates the existence of Alfvén waves inside the studied ICME flux rope. Moreover, we observed  $\theta_{VB} < 40^\circ$ , which implies the parallel propagation of AIC waves. We restricted ourselves as this wave is quasi-parallel in nature (He et al. 2011a; Telloni 2020) though many simulations and observation studies in the literature defined this wave as oblique in nature (Lacombe & Belmont 1995; Harmon & Coles 2005; He et al. 2011b; Isenberg & Vasquez 2011; Maneva et al. 2015).

Moreover, low-resolution data are sometimes not effective at measuring high-frequency fluctuations. The high-resolution data provides a more complete picture of the role of such

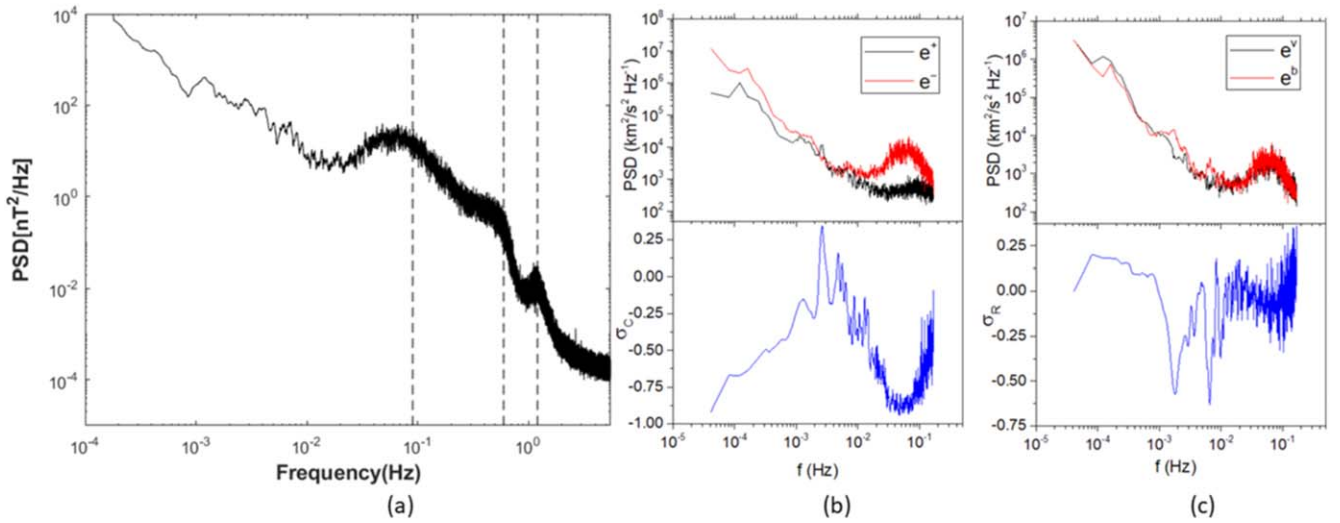


**Figure 4.** Panel (a) shows the spectral analysis of trace of magnetic field ( $\text{PSD}(B_x) + \text{PSD}(B_y) + \text{PSD}(B_z)$ ). Top part of panel (b) demonstrates spectral analysis  $e^+$  and  $e^-$ ; in addition, bottom part shows the variation of  $\sigma_c$  in the frequency domain. In the top part of panel (c), PSD of  $e^v$  and  $e^b$  is plotted along with that in the bottom part, where variation of  $\sigma_r$  is shown.

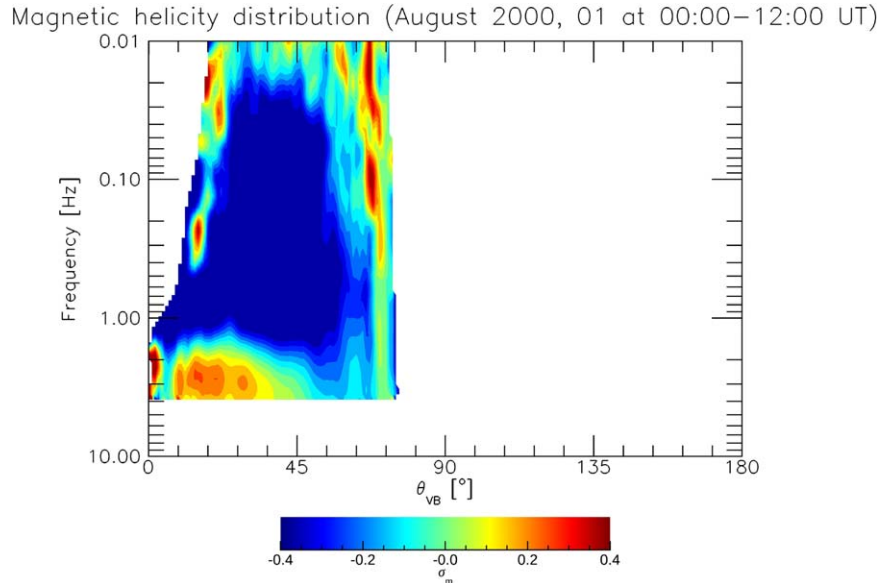


**Figure 5.** The normalized magnetic helicity spectrum,  $\sigma_m$ , is represented in color within this composite figure. It is plotted at various evenly spaced angles,  $\theta_{VB}$ , and combined to create the final visualization. Each vertical slice in the figure corresponds to the spectrum  $\sigma_m$  at a specific look angle,  $\theta_{VB}$ , relative to the local mean magnetic field direction.

high-frequency fluctuations in an ordered magnetic field. In the presence of turbulence, Alfvén waves can interact with one another and other types of waves, such as ICWs, to form an energy transfer cascade. This cascade can lead to the generation of AIC waves. The mechanism for this interaction involves a nonlinear wave–wave interaction process known as the parametric decay instability (Spangler et al. 1997), where an Alfvén wave can decay into two other waves with different frequencies and wavevectors.

The result of our analysis shown in Figure 3 supports the existence of Alfvén waves for the frequency range of ( $10^{-3}$  to  $10^{-1}$  Hz). Moreover, the estimation demonstrated in Figure 5 suggests ICWs (0.1 Hz to 1 Hz) coexist within the analyzed MCs. The coupling of fluid and kinetic scales gives us a clear and comprehensive picture of the kinetic processes underlying the generation of AIC waves in the ICME flux rope. This work














strongly provides observational evidence for the generation of left-hand-polarized parallel-propagating AICs and follow their anisotropic nonlinear turbulent cascade in the ICME flux rope driven by temperature anisotropy. We found the energy exchange between wave and particle at the gyrofrequency. Moreover, a perpendicular signature is much more effective for generating such waves.

### Acknowledgments

We acknowledge the use of the OmniWeb (or CDAWeb or ftp) service and OMNI data provided by the Space Physics Data Facility of NASA/GSFC. We thank SERB, India, whose project reference file number is CRG/2020/002314, supports AR and OD. Thanks to the Department of Physics (Autonomous) University of Mumbai, which provided the resources we

needed to complete this work. We also acknowledge Prof. Roberto Bruno for valuable suggestions.

### ORCID iDs

Omkar Dhamane  <https://orcid.org/0000-0002-4862-4141>  
 Vinit Pawaskar  <https://orcid.org/0009-0006-6848-9641>  
 Anil Raghav  <https://orcid.org/0000-0002-4704-6706>  
 Zubair Shaikh  <https://orcid.org/0000-0002-9206-6327>  
 Kalpesh Ghag  <https://orcid.org/0000-0002-9506-6875>  
 Kishor Kumbhar  <https://orcid.org/0009-0008-8804-0133>  
 Daniele Telloni  <https://orcid.org/0000-0002-6710-8142>  
 Georgios Nicolaou  <https://orcid.org/0000-0003-3623-4928>  
 Prathmesh Tari  <https://orcid.org/0009-0008-2630-0892>  
 Robert Wicks  <https://orcid.org/0000-0002-0622-5302>  
 Utsav Panchal  <https://orcid.org/0000-0003-2398-0438>  
 Bhagyashri Sathe  <https://orcid.org/0009-0003-1169-0748>  
 Prachi Pathare  <https://orcid.org/0009-0003-4949-2499>

### References

- Ala-Lahti, M., Kilpua, E. K., Souček, J., Pulkkinen, T. I., & Dimmock, A. P. 2019, *JGRA*, **124**, 3893
- Ala-Lahti, M. M., Kilpua, E. K., Dimmock, A. P., et al. 2018, *AnGeo*, **36**, 793
- Alexandrova, O., Chen, C. H. K., Sorriso-Valvo, L., Horbury, T. S., & Bale, S. D. 2013, *SSRv*, **178**, 101
- Anderson, B. J., Erlanson, R. E., & Zanetti, L. J. 1992, *JGR*, **97**, 3089
- Araneda, J. A., & Gomberoff, L. 2004, *JGRA*, **109**, A011006
- Araneda, J. A., Marsch, E., Adolfo, F., et al. 2008, *PhRvL*, **100**, 125003
- Behannon, K. 1976, PhD thesis, Catholic Univ. of America
- Belcher, J., & Davis, L., Jr 1971, *JGR*, **76**, 3534
- Belcher, J. W., & Solodyna, C. V. 1975, *JGR*, **80**, 181
- Blanco-Cano, X., Kajdič, P., Aguilar-Rodríguez, E., et al. 2016, *JGRA*, **121**, 992
- Bruno, R., & Carbone, V. 2013, *LRSP*, **10**, 2
- Bruno, R., & Trenchi, L. 2014, *ApJL*, **787**, L24
- Chang, T., Crew, G., Hershkowitz, N., et al. 1986, *GeoRL*, **13**, 636
- Coleman, P. J., Jr 1968, *ApJ*, **153**, 371
- Cramer, N. F. 2011, *The Physics of Alfvén Waves* (New York: Wiley)
- Davidson, R., & Ogden, J. M. 1975, *PhFI*, **18**, 1045
- Dhamane, O., Azmi, N., Manjrekar, A., et al. 2023a, *ApJ*, **945**, 64
- Dhamane, O., Raghav, A., Shaikh, Z., et al. 2023b, *SoPh*, **298**, 34
- Dusenbery, P. B., & Hollweg, J. V. 1981, *JGR*, **86**, 153
- Eyink, G. L., & Sreenivasan, K. R. 2006, *RvMP*, **78**, 87
- Franci, L., Verdini, A., Matteini, L., Landi, S., & Hellinger, P. 2015, *ApJL*, **804**, L39
- Gary, S. P., McKean, M. E., Winske, D., et al. 1994, *JGR*, **99**, 5903
- Goldstein, M., Roberts, D., & Fitch, C. 1994, *JGR*, **99**, 11519
- Gomberoff, L. 2003, *JGRA*, **108**, 1261
- Gomberoff, L., Hoyos, J., Brinca, A., & Ferrer, R. 2004, *JGRA*, **109**, A07108
- Gosling, J., McComas, D., Roberts, D., & Skoug, R. 2009, *ApJL*, **695**, L213
- Gosling, J., Teh, W.-L., & Eriksson, S. 2010, *ApJL*, **719**, L36
- Grappin, R., Frisch, U., Pouquet, A., & Leorat, J. 1982, *A&A*, **105**, 6
- Grappin, R., Velli, M., & Mangeney, A. 1991, *AnGeo*, **9**, 416
- Hanson, B., & Voss, D. 2007, *Sci*, **318**, 1571
- Harmon, J. K., & Coles, W. A. 2005, *JGRA*, **110**, A03101
- He, J., Marsch, E., Tu, C., Yao, S., & Tian, H. 2011a, *ApJ*, **731**, 85
- He, J., Tu, C., Marsch, E., & Yao, S. 2011b, *ApJL*, **745**, L8
- Hellinger, P., Trávníček, P., Kasper, J. C., & Lazarus, A. J. 2006, *GeoRL*, **33**, L09101
- Hollweg, J. V., Esser, R., & Jayanti, V. 1993, *JGR*, **98**, 3491
- Hollweg, J. V., & Isenberg, P. A. 2002, *JGRA*, **107**, 1147
- Hollweg, J. V., & Turner, J. M. 1978, *JGR*, **83**, 97
- Horbury, T., Wicks, R., & Chen, C. 2012, *SSRv*, **172**, 325
- Howard, T. 2011, *Coronal mass ejections: An introduction*, Vol. 376 (New York: Springer)
- Howard, T. A., & Tappin, S. J. 2009, *SSRv*, **147**, 31
- Isenberg, P. A., & Vasquez, B. J. 2011, *ApJ*, **731**, 88
- Jian, L. K., Russell, C. T., Luhmann, J. G., et al. 2010, *JGRA*, **115**, A12115
- Jian, L., Wei, H., Russell, C., et al. 2014, *ApJ*, **786**, 123
- Jian, L. K., Russell, C. T., Luhmann, J. G., et al. 2009, *ApJL*, **701**, L105
- Johnson, J. R., & Cheng, C.-Z. 1999, *GeoRL*, **26**, 671
- Kajdič, P., Blanco-Cano, X., Aguilar-Rodríguez, E., et al. 2012, *JGRA*, **117**, A06103
- Kilpua, E. K. J., Hietala, H., Koskinen, H. E. J., Fontaine, D., & Turc, L. 2013, *AnGeo*, **31**, 1559
- Kindel, J. M., & Kennel, C. 1971, *JGR*, **76**, 3055
- Kiyani, K. H., Osman, K. T., & Chapman, S. C. 2015, *RSPTA*, **373**, 20140155
- Knipp, D. J., McQuade, M. K., & Kirkpatrick, D. 2011, *Understanding Space Weather and the Physics behind it* (Learning Solutions) (New York: McGraw-Hill)
- Kunow, H., Crooker, N., Linker, J., et al. 2006, *Coronal Mass Ejections* (New York: Springer)
- Lacombe, C., & Belmont, G. 1995, *AdSpR*, **15**, 329
- Lepping, R., Acuña, M., Burlaga, L., et al. 1995, *SSRv*, **71**, 207
- Li, H., Wang, C., Chao, J., & Hsieh, W. 2016, *JGRA*, **121**, 42
- Lin, R., Anderson, K., Ashford, S., et al. 1995, *SSRv*, **71**, 125
- Liu, Y., Richardson, J. D., Belcher, J. W., et al. 2006, *JGRA*, **111**, A12S0
- Manchester, W., Kilpua, E. K., Liu, Y. D., et al. 2017, *SSRv*, **212**, 1159
- Maneva, Y., Viñas, A. F., Moya, P. S., Wicks, R. T., & Poedts, S. 2015, *ApJ*, **814**, 33
- Marsch, E. 2006, *LRSP*, **3**, 1
- Marsch, E., & Tu, C.-Y. 2001, *JGRA*, **106**, 227
- Ogilvie, K., Chornay, D., Fritzenreiter, R., et al. 1995, *SSRv*, **71**, 55
- Podesta, J. J., & Gary, S. P. 2011a, *ApJ*, **742**, 41
- Podesta, J. J., & Gary, S. P. 2011b, *ApJ*, **734**, 15
- Raghav, A., Dhamane, O., Shaikh, Z., et al. 2023, *ApJ*, **945**, 64
- Raghav, A., Shaikh, Z., Dhamane, O., et al. 2022, arXiv:2209.05037
- Raghav, A. N., Chorgha, K., & Shaikh, Z. I. 2019, *MNRAS*, **488**, 910
- Raghav, A. N., & Kule, A. 2018a, *MNRAS Lett.*, **476**, L6
- Raghav, A. N., & Kule, A. 2018b, *MNRAS Lett.*, **480**, L6
- Raghav, A. N., Kule, A., Bhaskar, A., et al. 2018, *ApJ*, **860**, 26
- Remya, B., Tsurutani, B., Reddy, R., et al. 2014, *ApJ*, **793**, 6
- Richardson, I. G., & Cane, H. V. 2004, *JGRA*, **109**, A09104
- Roberts, D. A., Goldstein, M. L., & Klein, L. W. 1990, *JGR*, **95**, 4203
- Roberts, D. A., Klein, L. W., Goldstein, M. L., & Matthaeus, W. H. 1987, *JGR*, **92**, 11021
- Schwartz, S. J., Burgess, D., & Moses, J. J. 1996, *AnGeo*, **14**, 1134
- Shaikh, Z. I., Raghav, A., & Vichare, G. 2019a, *MNRAS*, **490**, 1638
- Shaikh, Z. I., Raghav, A., Vichare, G., et al. 2019b, *MNRAS*, **490**, 3440
- Shaikh, Z. I., & Raghav, A. N. 2022, *ApJ*, **938**, 146
- Shaikh, Z. I., Raghav, A. N., Vichare, G., Bhaskar, A., & Mishra, W. 2020, *MNRAS*, **494**, 2498
- Siu-Tapia, A., Blanco-Cano, X., Kajdič, P., et al. 2015, *JGRA*, **120**, 2363
- Soucek, J., Escoubet, C. P., & Grison, B. 2015, *JGRA*, **120**, 2838
- Spangler, S. R., Leckband, J. A., & Cairns, I. H. 1997, *PhPI*, **4**, 846
- Stix, T. H. 1962, *The Theory of Plasma Waves* (New York: McGraw-Hill)
- Tajima, T., Mima, K., & Dawson, J. 1977, *PhRvL*, **39**, 201
- Telloni, D. 2020, *Atmos*, **12**, 44
- Telloni, D., & Bruno, R. 2016, *MNRAS Lett.*, **463**, L79
- Telloni, D., Bruno, R., D'Amicis, R., Pietropaolo, E., & Carbone, V. 2012, *ApJ*, **751**, 19
- Telloni, D., Bruno, R., & Trenchi, L. 2015, *ApJ*, **805**, 46
- Telloni, D., Carbone, F., Bruno, R., et al. 2019, *ApJL*, **885**, L5
- Telloni, D., Perri, S., Bruno, R., Carbone, V., & Amicis, R. 2013, *ApJ*, **776**, 3
- Thorne, R. M., & Horne, R. B. 1994, *JGR*, **99**, 17275
- Tsurutani, B. T., Arballo, J. K., Mok, J., et al. 1994, *GeoRL*, **21**, 633
- Tu, C.-Y., & Marsch, E. 1995, *SSRv*, **73**, 1
- Tu, C.-Y., Marsch, E., & Thieme, K. M. 1989, *JGR*, **94**, 11739
- Tu, C.-Y., Pu, Z.-Y., & Wei, F.-S. 1984, *JGR*, **89**, 9695
- Vlahos, L., & Cargill, P. 2009, *Turbulence in Space Plasmas*, Vol. 778 (Berlin: Springer)
- Walén, C. 1944, *ArMAF*, **30**, 1
- Webb, D. F., & Howard, T. A. 2012, *LRSP*, **9**, 3
- Wei, H., Jian, L., Russell, C., & Omid, N. 2016, in *Low-Frequency Waves in Space Plasmas*, ed. A. Keiling, D.-H. Lee, & V. Nakariakov (New York: Wiley), 253
- Wicks, R., Alexander, R., Stevens, M., et al. 2016, *ApJ*, **819**, 6
- Yang, L., & Chao, J. 2013, *ChJSS*, **33**, 353
- Yang, L., Lee, L., Chao, J., et al. 2016, *ApJ*, **817**, 178
- Zhao, G., Feng, H., Wu, D., Chu, Y., & Huang, J. 2017, *ApJL*, **847**, L8
- Zhao, G., Feng, H., Wu, D., Pi, G., & Huang, J. 2019, *ApJ*, **871**, 175
- Zimbardo, G., Greco, A., Sorriso-Valvo, L., et al. 2010, *SSRv*, **156**, 89
- Zurbuchen, T. H., & Richardson, I. G. 2006, *Coronal Mass Ejections*, Vol. 31 (New York: Springer)